PHYSICAL REVIEW B **91**, 140404(R) (2015)

Spinon confinement in the one-dimensional Ising-like antiferromagnet $SrCo_2V_2O_8$

Zhe Wang,[1,*] M. Schmidt,[1] A. K. Bera,[2,*] A. T. M. N. Islam,[2] B. Lake,[2,3] A. Loidl,[1] and J. Deisenhofer[1]

[1]*Experimental Physics V, Center for Electronic Correlations and Magnetism, Institute of Physics, University of Augsburg, 86135 Augsburg, Germany*

[2]*Helmholtz-Zentrum Berlin für Materialien und Energie, 14109 Berlin, Germany*

[3]*Institut für Festkörperphysik, Technische Universität Berlin, 10623 Berlin, Germany*

(Received 9 December 2014; published 9 April 2015)

For quasi-one-dimensional quantum spin systems theory predicts the occurrence of a confinement of spinon excitation due to interchain couplings. Here we investigate the system $SrCo_2V_2O_8$, a realization of the weakly coupled Ising-like XXZ antiferromagnetic chains, by terahertz spectroscopy with and without applied magnetic field. At low temperatures a series of excitations is observed, which split in a Zeeman-like fashion in an applied magnetic field. These magnetic excitations are identified as the theoretically predicted spinon-pair excitations. Using a one-dimensional Schrödinger equation with a linear confinement potential imposed by weak interchain couplings, the hierarchy of the confined spinons can be fully described.

DOI: 10.1103/PhysRevB.91.140404 PACS number(s): 75.30.−m, 71.70.Ej, 75.10.Pq

Confinement of quasiparticles, a phenomenon mostly known from particle physics [1], can be also realized in condensed matter [2–4]. Due to the strong interaction, quarks in a meson are asymptotically free at a shorter distance and never exist as individual particles. The counterpart in a condensed matter magnetic quasiparticle (spinon) exhibits similar confinement behavior. The spinon confinement can be illustrated in a paradigmatic one-dimensional system, the Ising-like XXZ spin-1/2 chain, where detailed theoretical descriptions have been achieved. In a single Ising chain, two spinons (domain walls) are created by a spin flip. The spinons, each carrying spin-1/2, can move freely along the chain by subsequent spin flips without cost of energy. This results in a highly degenerate first excited state with energy J, the intrachain nearest-neighbor exchange interaction. A finite transverse component of the exchange interaction lifts the degeneracy of the first excited states, leading to an excitation continuum composed of two spinons which propagate independently [5]. In the presence of weak interchain interactions, two spinons are bound because the separation between them will frustrate interchain interactions [Figs. 1(b) and 1(d)]. The interchain interaction plays the role of an attractive potential, proportional to the distance, confining the spinons into pairs. This leads to a quantization of the excitation continuum into discrete levels of spinon bound states [Fig. 1(e)].

In this Rapid Communication, we demonstrate experimentally such spinon confinement in the weakly coupled spin-1/2 Ising-like antiferromagnetic chain $SrCo_2V_2O_8$ by high resolution terahertz spectroscopy. $SrCo_2V_2O_8$ crystallizes in a tetragonal structure with the space group $I4_1cd$. The screw spin chains in $SrCo_2V_2O_8$, consisting of edge-sharing CoO_6 octahedra, propagate along the crystalline c axis, as shown in Figs. 1(a) and 1(b) [6,7]. Weak interchain couplings stabilize long-range collinear antiferromagnetic order below $T_N = 5$ K [6]. Spin-orbit coupling entangles the orbital and spin degrees of freedom of Co^{2+}, making the total angular momentum a conserved quantity. In the distorted octahedral environment, the lowest-lying Kramers doublet of Co^{2+} is well separated from the higher-lying spin-orbit quartet and sextet. Thus, the magnetic moment of Co^{2+} can be described by a highly anisotropic total angular moment with *pseudospin* $\tilde{S} = 1/2$ [8]. Significant Ising-like anisotropy along the c axis [Fig. 1(d)] is also achieved by cooperative effects of the crystal field splitting and spin-orbit coupling.

Intrachain exchange interactions between the pseudospins in $SrCo_2V_2O_8$ can be modeled by the Ising-like XXZ Hamiltonian [9]

$$J \sum_i \left[\tilde{S}_i^z \tilde{S}_{i+1}^z + \epsilon \left(\tilde{S}_i^x \tilde{S}_{i+1}^x + \tilde{S}_i^y \tilde{S}_{i+1}^y \right) \right], \qquad (1)$$

where $J > 0$ is the nearest-neighbor antiferromagnetic exchange interaction, and $0 < \epsilon < 1$ takes into account the Ising-like anisotropy arising from distortions of the CoO_6 octahedra.

High-quality single crystals of $SrCo_2V_2O_8$ were grown in Helmholtz-Zentrum Berlin (HZB) using the floating-zone method as described in Ref. [6]. Time-domain terahertz (THz) transmission measurements were performed in the spectral range 0.1–3.3 THz using a TPS Spectra 3000 spectrometer (TeraView Ltd.). Reference and samples were measured as a function of temperature. Power spectra were obtained by Fourier transformation of the time-domain signals. Magnetic-field-dependent transmission experiments were performed in Voigt geometry with backward wave oscillators covering frequencies from 0.32 to 1.4 THz and a magneto-optical cryostat (Oxford Instruments/Spectromag) with applied magnetic fields up to 3 T. Single crystals with a typical size $4 \times 4 \times 0.5$ mm^3 were aligned with respect to the crystalline a and c axes.

In Fig. 2(a) we show the electric-field amplitude of the transmitted electromagnetic wave through a reference and a $SrCo_2V_2O_8$ sample as a function of time delay in the magnetically ordered phase at 3.4 K. The incident light propagating along the crystalline a axis ($k \parallel a$) is polarized with the ac electric field parallel to the c axis ($e^\omega \parallel c$) and the ac magnetic field parallel to the a axis ($h^\omega \parallel a$). The transmission spectrum in the frequency domain [Fig. 2(b)] is

*Corresponding authors: zhe.wang@physik.uni-augsburg.de; anup.bera@helmholtz-berlin.de

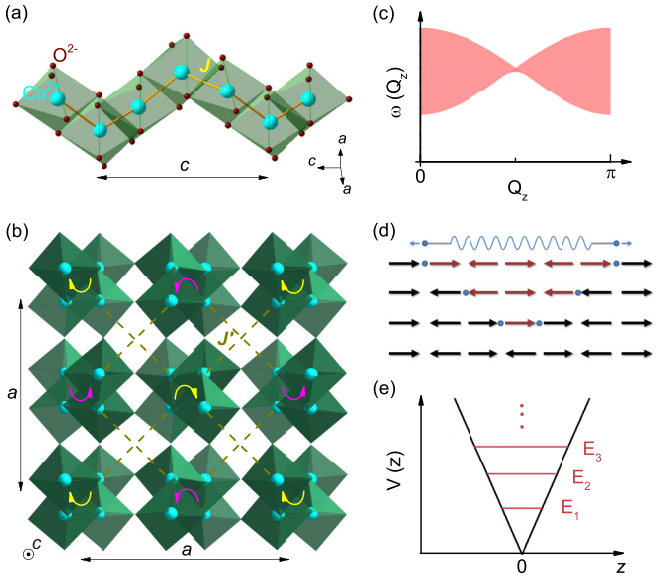

FIG. 1. (Color online) (a) Screw chain consisting of CoO_6 octahedra running along the crystalline c axis in $SrCo_2V_2O_8$. (b) Projection of left- and right-handed screw chains in the tetragonal ab plane. The interchain exchange interaction is dominated by the antiferromagnetic interaction J' between the nearest-neighbor Co ions in the ab plane, which are from the neighboring chains with the same chirality. (c) The shaded area indicates the excitation continuum of the spinon-pair quasiparticles corresponding to the Ising-like XXZ Hamiltonian in Eq. (1) [10]. The spinon pairs follow a quadratic dispersion relation along the chain direction close to the reciprocal Γ point ($Q_z = 0$) [5,10]. (d) Magnetic excitations of spinon pairs with total pseudospin $\tilde{S} = 1$ corresponding to an odd number of pseudospin-1/2 flips. The collinear antiferromagnetic order along the c axis is stabilized below 5 K [6]. (e) Quantized spinon-pair excitation levels due to linear confinement imposed by interchain exchange interaction.

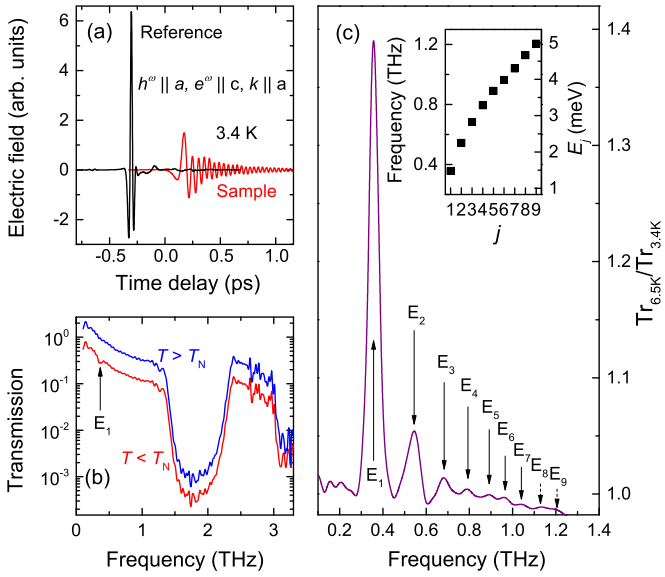

FIG. 2. (Color online) (a) THz time-domain signals of a reference and a $SrCo_2V_2O_8$ sample measured at 3.4 K with the ac magnetic field $h^\omega \parallel a$, the electric field $e^\omega \parallel c$, and the wave vector $k \parallel a$. (b) Transmission spectrum below and above T_N in the THz spectral range obtained from Fourier transformation of the time-domain signal. The spectrum measured above T_N is shifted upward for clarity. A dip corresponding to E_1 is marked in the spectrum measured below T_N. The spectral range from 1.3 to 2.3 THz and above 3 THz is dominated by broad phonon bands. (c) Ratio of transmission as obtained at 6.5 and 3.4 K as a function of frequency below the phonon band. Nine peaks can be observed and are indexed from E_1 to E_9. Excitation energy E_j vs energy level index $j = 1,2,3,\ldots$ is shown in the inset.

obtained by Fourier transformation of the time-domain signal. From the power spectrum measured below T_N, one can notice an absorption line at about 0.35 THz, marked as E_1. This absorption line is not observed above T_N. Figure 2(c) shows the power spectrum at 6.5 K right above T_N divided by the one measured at 3.4 K. One can readily observe the sharp line E_1 followed by a series of absorption lines $E_2, E_3, \ldots, E_9$ with increasing energies. These absorption lines are not observed when the ac magnetic field is parallel to the spin direction ($h^\omega \parallel c$). This points to the magnetic nature of the absorption modes. These modes can be assigned to magnetic excitations also based on their dependence on an external magnetic field, as discussed in the following.

The transmission spectrum of a monochromatic THz electromagnetic wave is measured at 2 K as a function of applied magnetic field along the chain direction, which is also the direction of the Ising-like spins in the magnetically ordered phase [6]. Typical spectra are shown in Fig. 3(a). Several absorption modes can be observed at the resonance fields in the spectrum of each frequency. The resonance magnetic fields shift with the frequencies of the electromagnetic waves. The absorption frequencies versus the corresponding resonance magnetic fields are plotted in Fig. 3(c). One can clearly recognize a series of absorption modes, which are split in the magnetic field, with energies increasing or decreasing with increasing magnetic field. All the lines follow a similar linear field dependence that can be described by a Zeeman interaction term $\pm g_\parallel \mu_B H \tilde{S}$, with a single value for the g factor, $g_\parallel = 5.5$, μ_B the Bohr magneton, and H the applied longitudinal magnetic field. The total pseudospin $\tilde{S} = 1$ has been used due to the fact that two spinons, each with $\tilde{S} = 1/2$, are involved. The plus or minus signs correspond to split modes in the magnetic field, and are also used to label the modes in Figs. 3(a) and 3(c). The zero-field energies obtained by extrapolating the linear field dependence to zero field are shown in Fig. 3(d). The zero-field spectrum of Fig. 2(c) is shown in Fig. 3(b) for comparison. The agreement in the energies for all observed excitations is clearly documented.

The observed magnetic excitations below T_N exhibit clear hierarchical features: The intensity of the lines decreases with increasing energy and the energy difference between neighboring excitations also decreases with increasing energy [see Fig. 2(c) and the inset]. These are exactly the features predicted by theory for spinon bound states due to confinement [11]. The excitations are indeed the spinon-pair excitations with total pseudospin $\tilde{S} = 1$, as confirmed by their field dependence. Every spinon-pair excitation is doubly degenerate in zero field, and the degeneracy is lifted in a finite longitudinal external magnetic field [Figs. 3(b) and 3(c)]. Energies of the

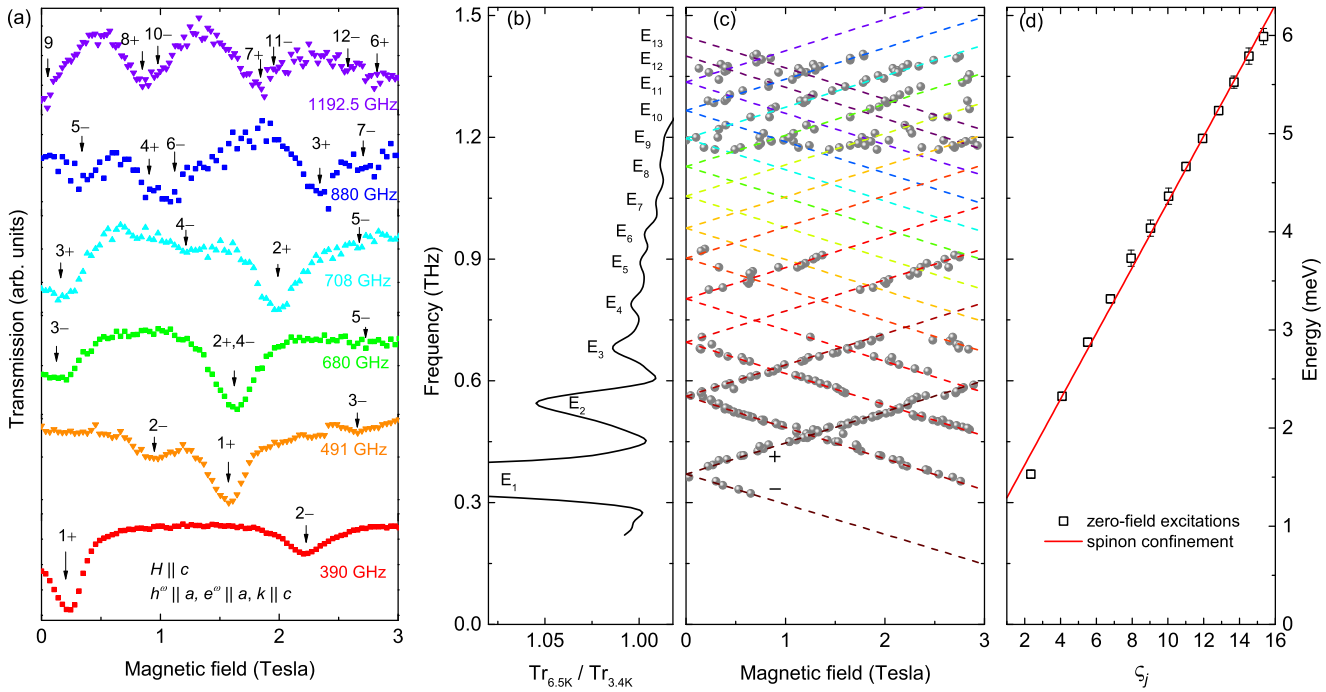

FIG. 3. (Color online) (a) Transmission spectra of various frequencies as a function of a longitudinal external magnetic field $H \parallel a$ at 2 K with the ac magnetic field $h^{\omega} \parallel a$, the electric field $e^{\omega} \parallel a$, and the wave vector $k \parallel c$. Absorption modes are marked by the corresponding number of the energy level in (b). (b) Normalized transmission spectrum at zero field adapted from Fig. 2(c). (c) Energies of absorption modes as a function of applied longitudinal magnetic field. Their field dependence can be described by a linear Zeeman term with a single g factor, $g_{\parallel} = 5.5$ (see text). (d) The hierarchy of the excitation energies at zero field can be modeled by the one-dimensional Schrödinger equation with linear confinement, Eq. (2). ζ_j's are the negative zeros of the Airy function (see text).

nondegenerate spinon-pair excitations increase or decrease depending on whether the total pseudospin is parallel or antiparallel to the external field, respectively.

The $\tilde{S} = 1$ spinon-pair bound states correspond to an odd number of pseudospin flips between the spinons, as illustrated in Fig. 1(d) [5,12]. The other series of spinon-pair excitations with $\tilde{S} = 0$ observed in $BaCo_2V_2O_8$ by neutron scattering experiments [13] are not observed in these THz measurements [see Fig. 3(c)]. This confirms the magnetic dipole active nature of the $\tilde{S} = 1$ spinon-pair excitations. For a spinon pair, the relative motion of one spinon with respect to the other along the chain can be described by the one-dimensional Schrödinger equation

$$-\frac{\hbar^2}{\mu}\frac{d^2\varphi}{dz^2} + \lambda|z|\varphi = (E - 2E_0)\varphi, \qquad (2)$$

with the linear potential $\lambda|z|$ taking into account the confinement imposed by the interchain antiferromagnetic exchange interaction J' [Fig. 1(b)], i.e., $\lambda = 2J'\langle\tilde{S}_z\rangle^2/c$. c is the lattice constant along the chain direction [Fig. 1(a)]. A quadratic dispersion relation at the Γ point has been assumed, following the calculations of the two-spinon dynamic structure factor [Fig. 1(b)] [10]. Since the photons have a linear dispersion relation with the speed of light involved, THz spectroscopy probes only the reciprocal space that is very close to the Γ point.

The solution of Eq. (2) gives the eigenenergies of the spinon-pair bound states [14],

$$E_j = 2E_0 + \zeta_j\lambda^{2/3}\left(\frac{\hbar^2}{\mu}\right)^{1/3}, \quad j = 1,2,3,\ldots. \qquad (3)$$

The sequence of the bound states is specified by the prefactors ζ_j that are the negative zeros of the Airy function $\mathrm{Ai}(-\zeta_j) = 0$, $\zeta_j = 2.338, 4.088, 5.520, \ldots$ $(j = 1,2,3,\ldots)$. $2E_0$ is the energy threshold for creating a free spinon pair. The bound-state energies at zero field exhibit a linear dependence on ζ_j, as shown in Fig. 3(d). The solid line in Fig. 3(d) is obtained by fitting the experimental results to Eq. (3). One can see that the energy hierarchy of the spinon-pair bound states is nicely modeled with $2E_0 = 0.96$ meV and $\lambda^{2/3}(\frac{\hbar^2}{\mu})^{1/3} = 0.33$ meV.

The energy threshold $2E_0$ is significantly smaller than the pure Ising-limit $J = 60\ \mathrm{K} \simeq 5.17$ meV. The value has been obtained by fitting the magnetic susceptibility using a pure Ising model [6,9]. The fact that $2E_0 \ll J$ stems from the finite ϵ term in Eq. (1) [5,10]. The deviation of ϵ from 1 is a measure of the anisotropy arising from distortions of the CoO_6 octahedra, which is also reflected by the $g_{\parallel}$ factor. If we assume a trigonal distortion with strength δ [15,16], then the induced anisotropy depends on the renormalized parameter δ/Λ, with $\Lambda < 0$ being the spin-orbit coupling. The obtained value of $g_{\parallel} = 5.5$ corresponds to $\delta/\Lambda = -0.80$ and $\epsilon = 0.73$ [15]. A smaller value of $\epsilon = 0.41$ in $BaCo_2V_2O_8$ indicates a larger distortion of the CoO_6 octahedra [13,15]. This is also indicated by a larger value of $g_{\parallel} = 6.2$ and a larger excitation gap of 1.7 meV in $BaCo_2V_2O_8$ with a similar intrachain exchange interaction [5,6,15,17,18].

Spinon bound states in the quasi-one-dimensional antiferromagnets $SrCo_2V_2O_8$ and $BaCo_2V_2O_8$ can be classified by their pseudospins, which are either $\tilde{S} = 1$ or $\tilde{S} = 0$, analogous to the classification of mesons (quark-antiquark bound states)

by their isospins (either 1 or 0). This is in clear distinction to the quasi-one-dimensional ferromagnet $CoNb_2O_6$ where the pseudospin is not a conserved quantity, since more spins are flipped at higher energies. Even at a certain energy level, spin blocks (domains) with different lengths in $CoNb_2O_6$ tend to flip with comparable probabilities [19].

In the strong interaction scenario, the strings between quarks can snap and heavy hadron particles are expected to decay into lighter ones, when creating heavier particles is energetically less favorable. Analogous to this scenario, spinon bound states can be expected only up to an energy of $E_1 + E_1$, above which an energy continuum would appear, as reported in $CoNb_2O_6$ [19]. This continuum is surprisingly not observed in $SrCo_2V_2O_8$ up to an energy much higher than $E_1 + E_1$. The difference is possibly due to the different strengths of spinon-spinon interactions in the two systems. The corresponding parameter $\lambda/\sqrt{\mu}$ in $SrCo_2V_2O_8$ is larger by one order of magnitude than in $CoNb_2O_6$. The $E_1 + E_1$ states with pseudospin $\tilde{S} = 2$ and any other bound states created by higher-order confinement processes with larger pseudospins, such as bound states of E_1 states in neighboring chains [19], can be excluded in $SrCo_2V_2O_8$, as documented in Fig. 3(c), because a stronger field dependence expected for these states is absent.

Using THz transmission spectroscopy also in external magnetic fields, we have investigated low-energy magnetic excitations in the quasi-one-dimensional Ising-like antiferromagnet $SrCo_2V_2O_8$. Spinon-pair excitations on the antiferromagnetic ground state have been observed in this XXZ-type antiferromagnet. Spinon-pair bound states with an entangled spin-orbit moment $\tilde{S} = 1$ are determined unambiguously. The hierarchy of the spinon-pair bound states can be described by a one-dimensional Schrödinger equation with a linear confinement potential imposed by the interchain interaction. An energy continuum of the elementary spinon-pair excitations is surprisingly not observed in $SrCo_2V_2O_8$.

We acknowledge helpful discussions with N. Peter Armitage. Partial support by the Deutsche Forschungsgemeinschaft via TRR 80 (Augsburg-Munich-Stuttgart) and by the Project DE 1762/2-1 is acknowledged.

[1] T. Muta, *Foundations of Quantum Chromodynamics* (World Scientific, Singapore, 1987).

[2] B. Lake, A. M. Tsvelik, S. Notbohm, D. A. Tennant, T. G. Perring, M. Reehuis, Ch. Sekar, G. Krabbes, and B. Büchner, Nat. Phys. **6**, 50 (2010).

[3] B. Lake, D. A. Tennant, and S. E. Nagler, Phys. Rev. Lett. **85**, 832 (2000).

[4] R. Coldea, D. A. Tennant, E. M. Wheeler, E. Wawrzynska, D. Prabhakaran, M. Telling, K. Habicht, P. Smeibidl, and K. Kiefer, Science **327**, 177 (2010).

[5] N. Ishimura and H. Shiba, Prog. Theor. Phys. **63**, 743 (1980).

[6] A. K. Bera, B. Lake, W.-D. Stein, and S. Zander, Phys. Rev. B **89**, 094402 (2014).

[7] Z. He, T. Taniyama, and M. Itoh, Phys. Rev. B **73**, 212406 (2006).

[8] A. Abragam and B. Bleaney, *Electron Paramagnetic Resonance of Transition Ions* (Clarendon Press, Oxford, UK, 1970).

[9] J. C. Bonner and M. E. Fisher, Phys. Rev. **135**, A640 (1964).

[10] A. H. Bougourzi, M. Karbach, and G. Müller, Phys. Rev. B **57**, 11429 (1998).

[11] H. Shiba, Prog. Theor. Phys. **64**, 466 (1980).

[12] J. P. Goff, D. A. Tennant, and S. E. Nagler, Phys. Rev. B **52**, 15992 (1995).

[13] B. Grenier, S. Petit, V. Simonet, E. Canévet, L.-P. Regnault, S. Raymond, B. Canals, C. Berthier, and P. Lejay, Phys. Rev. Lett. **114**, 017201 (2015).

[14] B. M. McCoy and T. T. Wu, Phys. Rev. D **18**, 1259 (1978).

[15] M. E. Lines, Phys. Rev. **131**, 546 (1963).

[16] A. Abragam and M. H. L. Pryce, Proc. R. Soc. London, Ser. A **206**, 173 (1951).

[17] S. Kimura, H. Yashiro, K. Okunishi, M. Hagiwara, Z. He, K. Kindo, T. Taniyama, and M. Itoh, Phys. Rev. Lett. **99**, 087602 (2007).

[18] Z. He, T. Taniyama, T. Kyômen, and M. Itoh, Phys. Rev. B **72**, 172403 (2005).

[19] C. M. Morris, R. Valdés Aguilar, A. Ghosh, S. M. Koohpayeh, J. Krizan, R. J. Cava, O. Tchernyshyov, T. M. McQueen, and N. P. Armitage, Phys. Rev. Lett. **112**, 137403 (2014).